Available online at www.sciencedirect.com
SCIENCE DIRECT®
ELSEVIER
Journal of Nuclear Materials 321 (2003) 19–28
journal of nuclear materials
www.elsevier.com/locate/jnucmat

Measured displacement energies of oxygen ions in titanates and zirconates

Katherine L. Smith [a,*], Michael Colella [a], Ronald Cooper [b], Eric R. Vance [a]

[a] *Materials Division, Australian Nuclear Science and Technology Organisation, PMB 1, 1 Illawarra Road, Lucas Heights, Menai, NSW 2234, Australia*

[b] *Department of Chemistry, University of Melbourne, Parkville, Vic. 3052, Australia*

Received 10 October 2002; accepted 17 March 2003

Abstract

Optical emission spectra in the 300–700 nm range were collected from four perovskite-structured materials ($CaTiO_3$, $SrTiO_3$, $BaTiO_3$ and $CaZrO_3$), a pyrochlore-structured material ($La_2Zr_2O_7$) and zirconolite ($CaZrTi_2O_7$), using either a Febetron 706 variable energy pulsed-electron-beam generator (pulse duration 3 ns) or a Vickers pulsed-electron LINAC (pulse duration 0.5 μs). The long-lived emissions (up to microseconds after the electron pulse) consist of broad (halfwidths ~100 nm) bands centred around ~400 nm. For the $CaZrO_3$, $La_2Zr_2O_7$ and $CaZrTi_2O_7$ samples, the emission intensity per unit dose was also measured as a function of electron beam energy over the range 0.2–0.6 MeV. The data for all three samples suggest a single stage dependence on electron beam energy. $CaZrO_3$, $La_2Zr_2O_7$, and $CaZrTi_2O_7$ have emission thresholds of 0.28 ± 0.03, 0.27 ± 0.03, and 0.26 ± 0.03 MeV respectively, which give oxygen displacement values of 49 ± 5, 47 ± 5, and 45 ± 5 eV respectively. Data collected in this study are discussed in the context of previously measured and calculated oxygen displacement values.

PACS: 61.72.Ji; 61.80.Fe; 61.82.Fk; 78.60.Hk

1. Introduction

The prevailing strategy for immobilising high level radioactive waste (HLW) is to incorporate it in a solid waste form and to eventually geologically isolate the waste form from the biosphere, after extended storage. Consequently, assessment of the long-term self-irradiation response of the solid and the effect of radiation damage on aqueous durability are critical issues.

In addition to borosilicate glass and ceramics, ceramic assemblages of titanate or alternatively zirconate phases have been proposed as HLW waste forms. Titanate waste form research started in 1978 [1] and has been almost continuous up to the present day (e.g. [2]). In 1998, this body of work resulted in the US government legislating to use a pyrochlore-rich titanate ceramic [3] to immobilise 17 metric tons of impure surplus plutonium. Subsequently, that decision was overturned for administrative reasons. Nevertheless, the essential viability of the titanate ceramics remains proven.

Published zirconate waste form research has been much more sporadic than titanate waste form research. In 1993, a zirconate waste form was shown to have comparable aqueous durability to titanate waste forms [4,5]. Then in 1999, synthetic single-phase gadolinium zirconate pyrochlore ($Gd_2Zr_2O_7$) was shown to be much more radiation resistant than the corresponding gadolinium titanate pyrochlore ($Gd_2Ti_2O_7$) [6]. In 2001, tests were conducted to ascertain the effects of replacing Ti by Zr in the baseline ceramic proposed for Pu disposition. The radiation resistance of the major zirconate phase (a defect fluorite) was at least 10 times greater than that of the corresponding Ti pyrochlore. However it was also

* Corresponding author. Tel.: +61-2 9717 3503; fax: +61-2 9543 7179.
E-mail address: kls@ansto.gov.au (K.L. Smith).

0022-3115/$ - see front matter
doi:10.1016/S0022-3115(03)00197-1

found that zirconate assemblages are much less chemically flexible than titanate assemblages [7].

Modelling of radiation damage effects requires accurate knowledge of the displacement energies of the atoms in the solid. Various techniques have been used to monitor defect production and/or expose the presence of pre-existing defects in irradiated non-metals. These include: (a) the detection of dislocation loops by transmission electron microscopy (TEM), (b) optical absorption and (c) time-resolved cathodoluminescence spectroscopy (TRCS). Zinkle and Kinoshita [8] collated all the E_d (oxygen) values for Al_2O_3 and MgO that had previously been measured by TEM (loop method), optical absorption and TRCS, and on that basis recommended usage of values that were within experimental error of those measured by TRCS. Recently, Cooper et al. [9] and Smith et al. [10] used time-resolved cathodoluminescence spectroscopy (TRCS) to measure the displacement energy (E_d) of oxygen ions in various titanate phases.

TRCS involves irradiating suitable samples with pulsed beams of fast electrons (>0.2 MeV) and monitoring the ultraviolet/visible luminescence produced by short-lived F-type centres whose lifetimes are negligible compared to the time between electron pulses. F-type centres are anion vacancies (F^{2+}) that contain one or two bound electrons (F^+ or F-centres respectively). Electron irradiation causes displacement of anions and a simultaneous production of excited F-type centres by electron trapping in the anion vacancy. Decay of the excited F-type centre releases characteristic photons. The process can be represented by:

$$F^{2+} + e \Rightarrow F^{+*}$$

$$F^{+*} \Rightarrow F^{+} + h\nu$$

where $*$ denotes an excited state. In this and previous Febetron-based TRCS studies, the durations of the electron beam pulses, F-centre life times and the time between pulses are ~3 ns, ~10 μs and >30 s respectively. It is important to note that the F centre lifetimes are negligible compared to the pulse frequency.

For relativistic particles such as electrons, the maximum energy T_m (in eV) transferable from an incident electron of energy E (in MeV) to a lattice ion of mass number A is given [11] by:

$$T_m = 2147.7E(E + 1.022)/A \quad (1)$$

Consequently, it is possible to determine whether or not atomic displacement occurs upon irradiation by monitoring the emission intensity per unit of absorbed dose as a function of incident electron energy. If a threshold is observed to occur at an incident electron energy E, then T_m is equal to the displacement energy E_d of the atom or ion in the lattice whose displacement gives rise to the short-lived F-centre.

Previous TRCS studies of CaO and sapphire (Al_2O_3), revealed transient characteristic emission bands, at 375 and 330 nm respectively, that were shown [12–14] to result from the relaxation of short-lived excited F^+ centres. More recently, Kotomin et al. [15] simulated various point defects in perovskite-structured $KNbO_3$ crystals using a semi-empirical method and measured the transient absorption spectra resulting from pulsed electron beam irradiation (electron beam energy 0.27 MeV, average excitation density during the irradiation pulse 15 MW/cm^{-2}, pulse duration 10 ns). Comparison of their theoretical and experimental results indicate electron irradiation produces transient excited F-centres in $KNbO_3$.

This paper reports TRCS investigations of four perovskites ($CaTiO_3$, $SrTiO_3$, $BaTiO_3$ and $CaZrO_3$), two pyrochlores ($Y_2Ti_2O_7$ and $La_2Zr_2O_7$) and zirconolite ($CaZrTi_2O_7$) and reviews these results in the context of previous results.

2. Experimental method

High-quality single crystals of $CaTiO_3$, $SrTiO_3$ and $BaTiO_3$, $1 \times 1 \times 10$ mm in size, were purchased from Escete (Netherlands). Polycrystalline samples of $CaTiO_3$, $CaZrO_3$, $Y_2Ti_2O_7$, $La_2Zr_2O_7$ and $CaZrTi_2O_7$ were made via the alkoxide/nitrate route [1] and sintered in air at temperatures between 1400 and 1500 °C for periods of between 24 and 48 h. Scanning electron microscopy (SEM) and X-ray diffraction (XRD) showed that all the polycrystalline samples are near single phase. TRCS was performed on both the single crystals and on specimens of the various polycrystalline samples, which were approximately $3 \times 0.5 \times 10$ mm in size.

2.1. Febetron experiments

A Febetron 706 (Hewlett Packard, Field Emission Division) pulsed electron beam generator was used to irradiate samples at room temperature. Single pulses of electrons of duration 3 ns (FWHM) with designated energies from 0.2 up to 0.6 MeV could be produced. The energy of the designated electron energies is accurate to within 5–10%. The relative dose per pulse delivered by the electron accelerator was calibrated at intervals over the energy range 0.2–0.6 MeV using a 'radiochromic' dosimetry technique [16]. The calibrations were fitted to an appropriate spline function, which was then used to interpolate doses at intermediate beam energies. The maximum output of the Febetron at 0.6 MeV is 12 J per pulse. The diameter of the electron beam was ~6 mm. Previous Febetron-based measurements on single crystal and polycrystalline $CaTiO_3$ perovskite [9] suggest that the cathodoluminescent emission in oxides is mostly derived from a surface layer no more than ~10 μm thick.

In the Febetron, samples were mounted with a flat face at 45° to the axis of the incident electron beam in an aluminium irradiation vessel centrally located in front of the electron beam window. The vessel was routinely evacuated to less than 10^{-3} Torr prior to irradiation, to eliminate emissions from various components in air (mainly N_2 and H_2O). These emissions occur in the 300–400 nm region of the spectrum and have comparable lifetimes (but not thresholds) to those anticipated for F-type luminescent defects.

Light emission from the Febetron sample was observed at 90° to the axis of the electron beam via a system of quartz lenses focussing onto the slits of a monochromator (Spex Industries, Minimate 1670). We collected two types of data. Firstly we irradiated the samples with 0.5 MeV electrons, and measured the intensity of the emitted light as a function of the wavelength of the emitted light. Henceforth we will call these 'intensity versus wavelength' spectra. These spectra give the positions of emission maxima. Secondly we monitored the light intensity at the emission maxima wavelength as a function of the energy of the incident electrons, as the energy of the incident electrons was varied from 0.2 to 0.6 MeV. Henceforth we will call these 'intensity versus energy' spectra. Typically, a bandpass of 2 nm was used to record intensity versus wavelength spectra, and 5 nm was used for intensity versus energy spectra. The latter spectra show thresholds and the wider bandpass allowed greater sensitivity at low electron beam energies. Individual data points displayed in the spectra reported in the paper represent the mean of between three and ten measurements. The output from the optical system was monitored with a photomultiplier, displayed on a digitising/digital oscilloscope and exported to a Macintosh PC for further analysis.

The electron beam pulses were 3 ns in duration and the rise time of the system was of the order of 10 ns. If the incident electrons had energies greater than the displacement threshold, light emission was observed immediately after the electron beam pulse. For all the samples in our previous studies [9,10] and all but the $La_2Zr_2O_7$ sample in this study, the shape of the plot of photon emission as a function of time after irradiation was sample independent and independent of the energy of the incident electrons. The measured photon emission from all samples except $La_2Zr_2O_7$ (a) peaked about 25 ns after electron irradiation, (b) showed a rapid initial decay over a period of 50 ns and (c) a long 'tail' which continued for many microseconds. This type of decay can be modelled using a power law (intensity is proportional to time^{-y}, where y is in the range 1–2).

At low incident electron energies (<~0.3 MeV), the emission response of $La_2Zr_2O_7$is similar to that of other oxides. At higher incident electron energies, the emission falls off more slowly with time. For example, Fig. 1 shows $La_2Zr_2O_7$ emission data taken using 0.44 MeV electrons from the Febetron. For any given energy of the incident electrons, the emission response of $La_2Zr_2O_7$ is independent of wavelength. Regardless of incident electron energy (0.2–0.6 MeV), all the photon emission spectra from $La_2Zr_2O_7$ show a large peak 25 ns after the electron pulse.

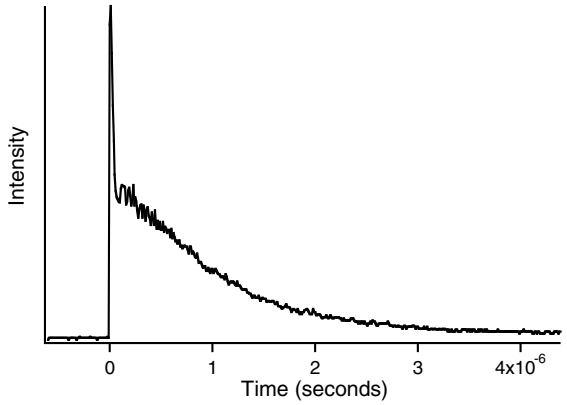

Fig. 1. Intensity of light emitted from a $La_2Zr_2O_7$ pyrochlore specimen irradiated at room temperature with 0.44 MeV electrons as a function of time.

As stated above, for all samples except $La_2Zr_2O_7$, the shape of the emission versus time after an electron pulse is independent of the energy of the incident electrons. Consequently for all samples except $La_2Zr_2O_7$, measurement of the intensity at a fixed time after the pulse is directly proportional to the integrated light yield. For all the samples in this study we chose to measure the intensity 25 ns after the electron beam pulse (i.e. at maximum intensity). For $La_2Zr_2O_7$ we also recorded data 150 ns after the electron beam pulse. The time between successive electron pulses was always greater than 30 s.

The positions of data points in the intensity versus wavelength spectra and the intensity versus energy spectra did not depend on the order in which data are taken. Consequently no permanent optically active defects were produced in our samples during electron irradiation.

2.2. LINAC experiments

A Vickers LINAC pulsed electron generator delivering 0.5 μs pulses of 15–20 MeV electrons was used to investigate the wavelength dependent cathodoluminescence from the three perovskite samples ($CaTiO_3$, $SrTiO_3$ and $BaTiO_3$) at high incident electron energies. The LINAC is situated at the Yallambie Laboratories of the Australian Radiation Protection and Nuclear Safeguards Agency (ARPANSA). The optical system was similar in design to that used in the Febetron experiments except that the samples were irradiated in air and

the temporal emission data at a given monochromator setting were recorded directly into a computer data acquisition system (ELACC). Emission was only recorded at times >0.5 μs after the electron pulse. The dose delivered was of the order of 5 J/kg per pulse.

3. Results

3.1. Perovskite data

In an earlier study, we used the Febetron to collect intensity versus wavelength spectra from $CaTiO_3$, $SrTiO_3$ and $BaTiO_3$ [9]. In the present study we used the LINAC (Fig. 2). The spectra we collected using the LINAC are essentially the same as those we collected using the Febetron despite the facts that (a) the signal to noise ratio of the LINAC is much higher than that of the Febetron and (b) the Febetron produces electrons with incident energies between 0.2 and 0.6 MeV while the LINAC produces electrons with incident energies between 15 and 20 MeV. The similarity of the results from the Febetron and LINAC indicate that F-centers are the only defects that produce optical emission.

Fig. 2(a) compares the wavelength versus intensity spectra of $CaTiO_3$, $SrTiO_3$ and $BaTiO_3$. The maximum emissions for $CaTiO_3$, $SrTiO_3$ and $BaTiO_3$ occur at around ~380, ~410 and ~430 nm respectively. There is clearly a distinct shift in maximum emission towards longer wavelengths as calcium is replaced with successively heavier alkaline earth cations. The shift in the maxima of the $CaTiO_3$, $SrTiO_3$ and $BaTiO_3$ intensity

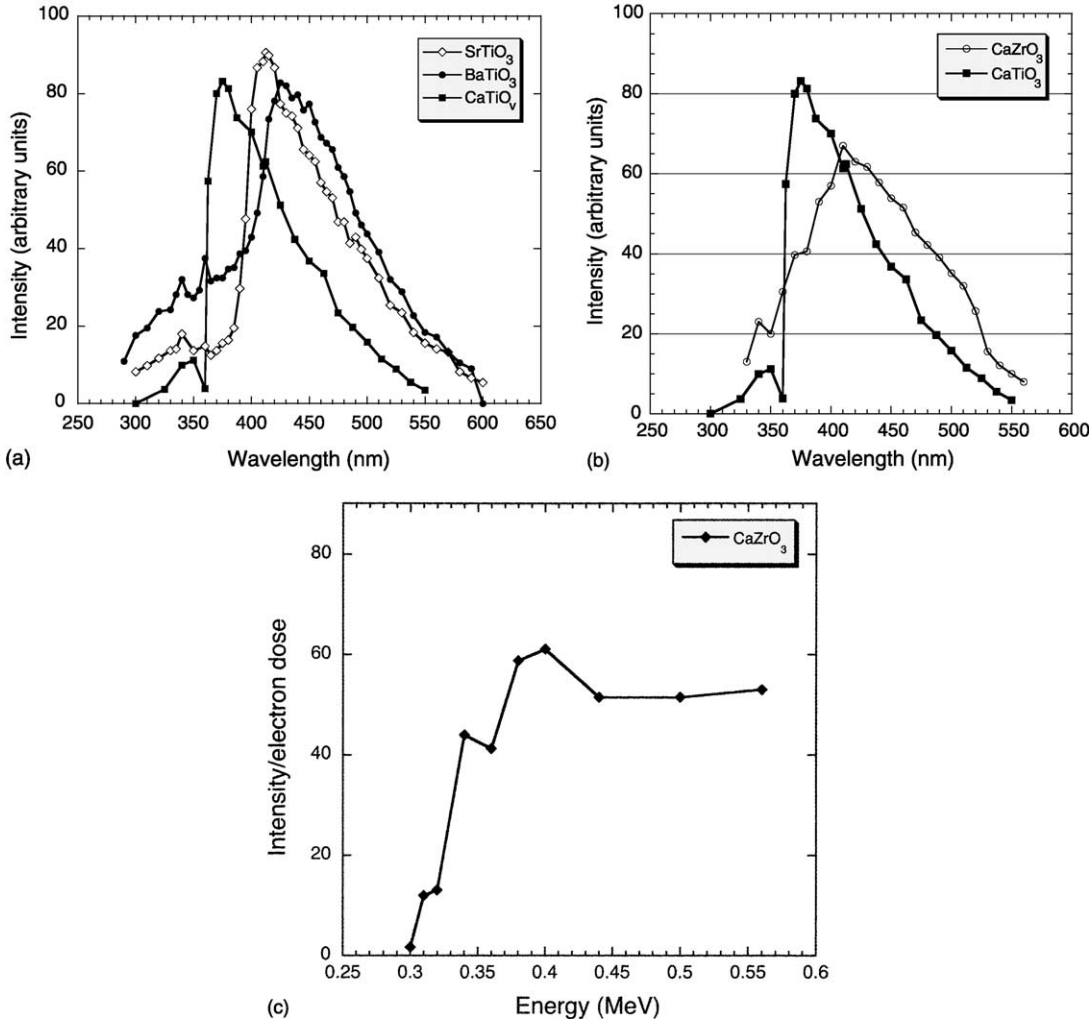

Fig. 2. (a) Room temperature luminescence spectra from $CaTiO_3$, $SrTiO_3$ and $BaTiO_3$. (b) Room temperature luminescence spectra from $CaTiO_3$ and $CaZrO_3$. (c) Graph of photon intensity emitted by $CaZrO_3$ at room temperature as a function of electron energy.

versus wavelength spectra (Fig. 2(a)) may reflect differences in the depth of the anion vacancy potential well arising from the increasing neighbouring cation size from calcium to barium.

The wavelength versus intensity spectra of $CaTiO_3$ and $CaZrO_3$ collected using the LINAC accelerator are compared in Fig. 2(b). The maximum emissions for $CaTiO_3$ and $CaZrO_3$ occur at around 380 and ~410 nm respectively. That is, there is a distinct shift in maximum emission towards longer wavelengths when titanium is replaced with zirconium. This is a similar effect to the shift in maxima observed for the Ca–Sr–Ba series above.

All the perovskites we have examined ($CaTiO_3$, $SrTiO_3$, $BaTiO_3$ and $CaZrO_3$) show broadly similar luminescence intensity versus wavelength spectra and decay kinetics. Furthermore they all exhibit similar emission thresholds. Consequently it is likely that the same defect (an excited F-centre) causes the observed cathodoluminescence in all cases.

Both Ti^{3+} and Ti^{4+} in alumina are well known to cause luminescence in the visible range [17] and it is possible that Ti^{3+} could be created in the titanate perovskites by electron irradiation. However we would not expect such a process to be characterised by a threshold energy of ~0.3 MeV.

Fig. 2(c) shows the emission intensity per unit dose of $CaZrO_3$ measured as a function of electron beam energy at 440 nm collected using the Febetron. These data show a single stage dependence of emission intensity per unit dose on electron beam energy over the range 0.2–0.6 MeV with a threshold of 0.30 ± 0.03 MeV.

3.2. $Y_2Ti_2O_7$ (pyrochlore) data

The $Y_2Ti_2O_7$ data in Fig. 3 have been published previously [18] and are re-presented here for comparison with new data for $La_2Zr_2O_7$. Fig. 3(a) shows a plot of emitted intensity from $Y_2Ti_2O_7$ versus wavelength, exhibiting a single broad (halfwidth ~100 nm) emission band centred around ~380 nm. Fig. 3(b) shows the emission intensity per unit dose from $Y_2Ti_2O_7$ as a function of electron beam energy collected at 380 nm. These data show a single stage dependence of emission intensity per unit dose on electron beam energy over the range 0.2–0.6 MeV and identify an emission threshold of 0.27 ± 0.03 MeV. All data in Fig. 3 were collected using the Febetron.

3.3. $La_2Zr_2O_7$ (pyrochlore) data

Fig. 4(a) shows the variation in light intensity emitted by $La_2Zr_2O_7$as a function of wavelength, 25 and 150 ns after the electron beam pulse measured using the Febetron. Both sets of data show a single broad (halfwidth ~100 nm) peak. For the data collected 25 ns after the electron beam pulse, the emission band is centred around ~430 nm with considerable intensity remaining at 500 nm. The data collected after 150 ns show a more symmetrical band centred on 460 nm. The difference spectrum in Fig. 4(a), calculated by subtracting the data collected 150 ns after the electron beam pulse from the data collected 25 ns after the electron beam pulse, is indicative that the species causing the fast decay component of the emission, has a maximum around 410 nm and shows little emission above 500 nm. This is similar to the spectra and decay kinetics of all the other oxides measured 25 ns after the electron dose.

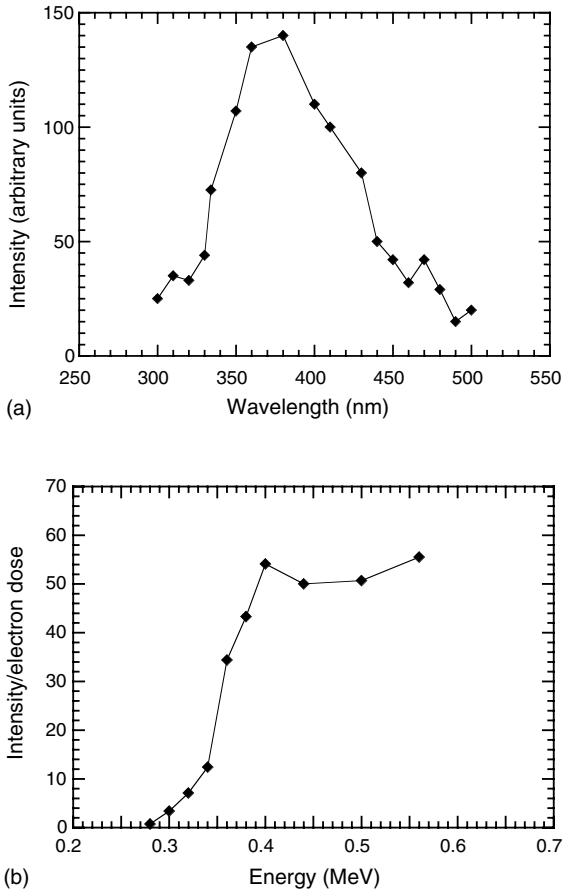

Fig. 3. (a) Room temperature luminescence spectra from $Y_2Ti_2O_7$. (b) Graph of photon intensity emitted by $Y_2Ti_2O_7$ at room temperature as a function of electron energy.

Fig. 4(b) shows the emission intensity per unit dose at 430 nm from $La_2Zr_2O_7$as a function of electron beam energy, taken at 25 and 150 ns after the electron beam pulse. Subtraction of these data sets separates the behaviour of the fast and slower components of the composite emission spectrum with respect to impacting electron energy. All three spectra in Fig. 4(b) have emission thresholds of 0.27 ± 0.03 MeV. The TRCS intensity per electron dose versus energy data for all oxides

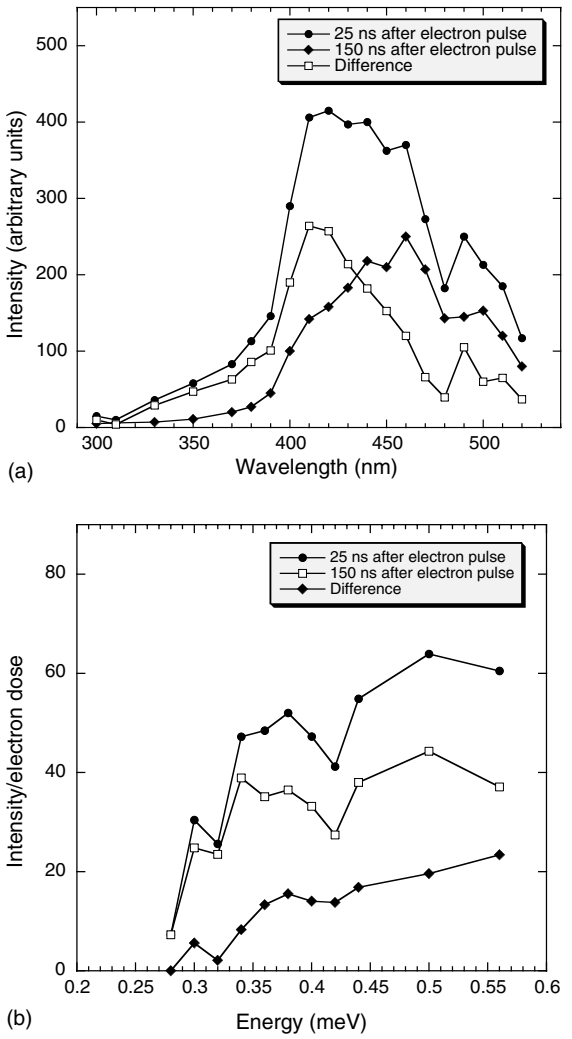

Fig. 4. (a) Room temperature luminescence spectra from $La_2Zr_2O_7$, taken 25 and 150 ns after the electron beam pulse and the difference spectrum calculated by subtracting the data collected at 150 ns after the electron pulse from the data collected 25 ns after the electron pulse. (b) Graphs of photon intensity emitted by $Y_2Ti_2O_7$ at room temperature as a function of electron energy taken at 25 and 150 ns after the electron beam pulse and the difference spectrum.

except $La_2Zr_2O_7$ show plateaux in intensity per electron dose. However the difference spectrum for $La_2Zr_2O_7$ in Fig. 4(b) shows a slow increase in emission yield with increasing electron energy that does not plateau even at the maximum energy used (0.58 MeV).

The fast decaying emission species in $La_2Zr_2O_7$ is likely to be an F^+-type centre, as with other oxides, for the following reasons.

- The initial decay kinetics of $La_2Zr_2O_7$ (<50 ns after the electron dose) are similar to those of other oxides.
- The difference spectra in Fig. 4(a) and (b) (which represent the behaviour of the fast decay species) are similar to those recorded for all other oxides 25 ns after the initial electron dose.
- All the curves in Fig. 4(b) have thresholds of 0.27 ± 0.03 MeV. This value is similar to the thresholds of other oxides and in particular is identical to that of $Y_2Ti_2O_7$ (which has the same structure as $La_2Zr_2O_7$).

The lack of a plateau in the difference data in Fig. 4(b) could indicate the presence of a defect species with a range of displacement cross sections or a range of defects rather than a single threshold value. However $Y_2Ti_2O_7$ (which has the same structure as $La_2Zr_2O_7$) does not show the same emission characteristics as $La_2Zr_2O_7$, so it is unlikely that there is more than one displacement energy for oxygen in perfectly crystalline $La_2Zr_2O_7$.

The identity of the slower decaying emission species in $La_2Zr_2O_7$ is as yet unknown. We considered the possibility that the slow decay emission was due to surface defects (e.g. oxygen depleted or strained sites) in our sample. So we heat-treated our sample (1200 °C for 24 h in air) and re-measured its cathodoluminescence. There were no significant differences before and after heat treatment. The threshold measurement for the slow decaying component shows an increase in intensity per unit dose as the energy of the impacting electrons increases. At higher energies penetration of the electron beam into the bulk of the crystal will be greater and hence surface effects will be relatively less important than at lower electron beam energies. The present observation supports the proposal that the slow decaying species being a surface site related emission. It may be possible that there is a small amount of an ancillary phase present in our $La_2Zr_2O_7$ sample that hosts the slower decaying emission species. However this is unlikely as all samples were checked for homogeneity using XRD and SEM. Additional samples known to contain contaminant phases would need to be made to fully explore the ancillary phase hypothesis, but that is beyond the scope of this study.

3.4. Zirconolite data

Fig. 5(a) shows the wavelength versus intensity spectrum of zirconolite collected in an earlier study [10]. On the basis of this data we previously suggested that the broad (halfwidth ~100 nm) emission band suggests the presence of two overlapping bands centred around ~380 and ~420 nm [10]. Fig. 5(b) and (c) shows the emission intensity per unit dose as a function of electron beam energy from zirconolite measured at 380 and 420 nm respectively. Both data sets in Fig. 5(b) and (c) show a single stage dependence of emission intensity per

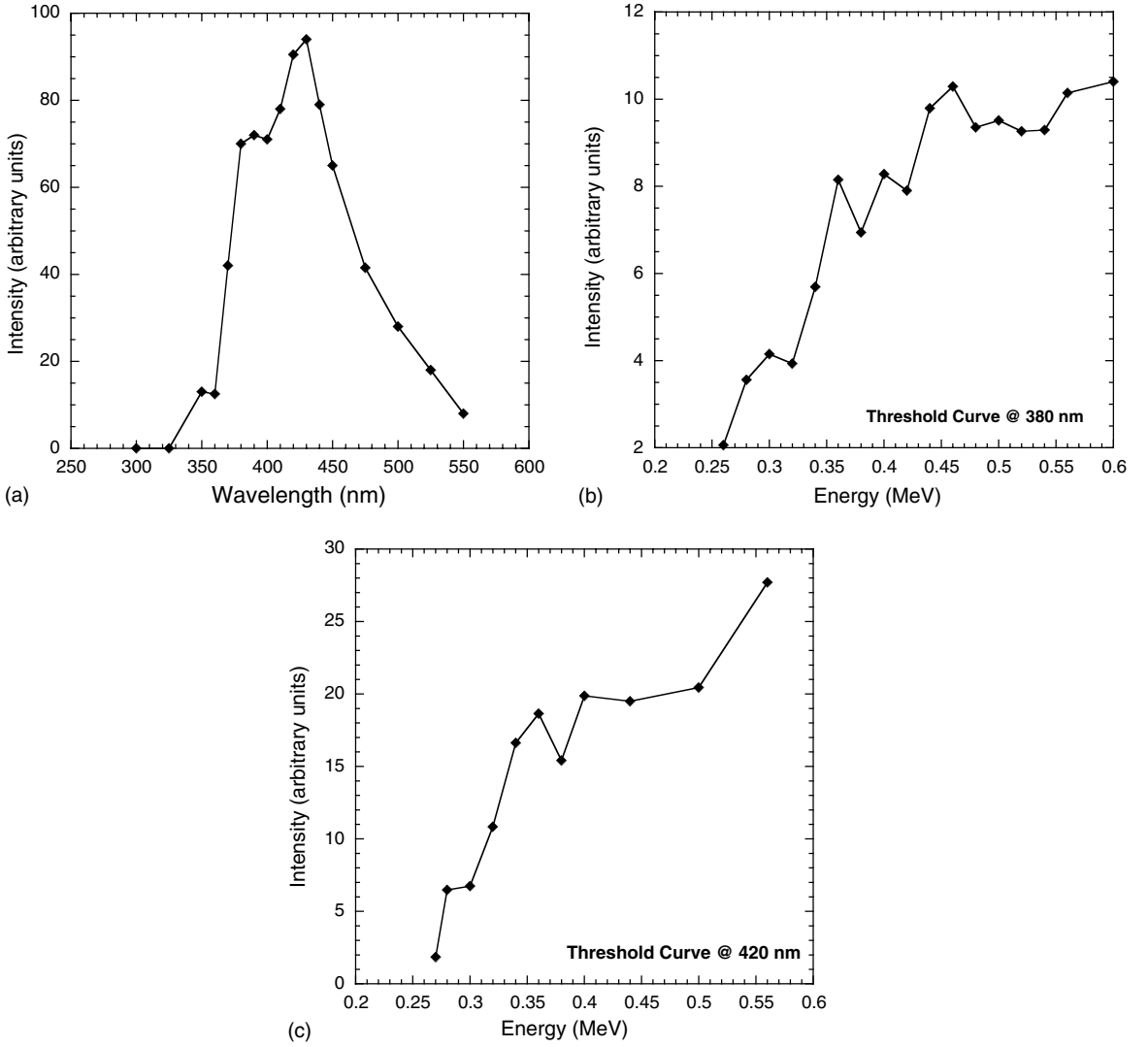

Fig. 5. (a) Room temperature luminescence spectra from zirconolite, $CaZrTi_2O_7$. (b) Graph of intensity of 380 nm photons emitted by electron irradiated zirconolite at room temperature as a function of electron energy. (c) Graph of intensity of 440 nm photons emitted by electron irradiated zirconolite at room temperature as a function of electron energy.

unit dose on electron beam energy over the range 0.2–0.6 MeV and an emission threshold of 0.26 ± 0.03 MeV. All data in Fig. 5 were collected using the Febetron.

3.5. E_d values

As stated above, the intensity versus energy spectra of $CaZrO_3$, $Y_2Ti_2O_7$ and $La_2Zr_2O_7$ show intensity thresholds at 0.30 ± 0.03 MeV, 0.27 ± 0.03 MeV and 0.27 ± 0.03 MeV respectively, while both of the zirconolite data sets show intensity thresholds of 0.26 ± 0.02 MeV. On the basis of Eq. (1) and assuming that the displaced ions in our samples are oxygen, we calculate oxygen displacement, E_d (oxygen), values of 53 ± 5 eV for $CaZrO_3$, 47 ± 5 eV for $Y_2Ti_2O_7$, 47 ± 5 eV for $La_2Zr_2O_7$ and 45 ± 5 eV for zirconolite. If one assumes the displaced ions are other than oxygen, Eq. (1) yields E_d values that are unrealistically low compared to experimental and calculated cation displacement energies in other oxides [8] (Table 1).

The fact that many of the E_d (oxygen) thresholds we have measured in this and previous studies cluster around 0.3 MeV is not an artefact of using TRCS and/or the specific Febetron we employed. The same techniques and Febetron showed a threshold value of 0.51 MeV for cadmium sulphide [19].

Table 1
Displacement energies (E_ds) for different ions calculated on the basis of our data

Compound Threshold (MeV)	$Y_2Ti_2O_7$ 0.27 ± 0.03	$La_2Zr_2O_7$ 0.27 ± 0.03	$CaZrO_3$ 0.30 ± 0.03	$CaZrTi_2O_7$ 0.26 ± 0.03
E_d assuming displaced ion is oxygen	47 ± 5	47 ± 5	53 ± 5	45 ± 5
E_d assuming displaced ion is yttrium	*8.4 ± 0.8*			
E_d assuming displaced ion is titanium	*16 ± 2*			*15 ± 2*
E_d assuming displaced ion is lanthanum		*5.4 ± 0.5*		
E_d assuming displaced ion is zirconium		*8.2 ± 0.8*	*9.3 ± 0.9*	*7.8 ± 0.8*
E_d assuming displaced ion is calcium			*21 ± 2*	*18 ± 2*

All the cation E_ds shown in italics are unrealistically low compared to previously measured experimental and calculated cation E_ds in oxides.

4. Discussion

During this and previous TRCS studies the following observations were made.

- All the oxides showed similar wavelength dependent cathodoluminescence (i.e. ~100 nm wide emission bands in the 350–500 nm region of the spectrum).
- All the oxides show similar (largely wavelength independent) cathodoluminescence decay characteristics (photon emission peaks about ~25 ns after electron irradiation, then falls off rapidly until ~50 ns after electron irradiation when the intensity reaches ~5% of maximum, and then emission tails off slowly for many microseconds).
- TRCS emission from $La_2Zr_2O_7$ is slightly different from that from other oxides in that it shows a strong second emission peak at longer wavelengths and a longer decay tail. However the emission from $La_2Zr_2O_7$ over the first 50 ns after electron dose is practically identical to that from other oxides. Both peaks have the same energy threshold. Consequently the second peak is also likely to be related to F-centre emission.
- All oxides have similar energy thresholds for cathodoluminescence.
- The E_d (oxygen) in these oxides ranges over approximately 20 eV, from 39 to 58 eV.

Structural characteristics and properties of various oxides are listed in Table 2. They include:

- the average number of cations coordinated to the oxygen site(s) (OCN)

Table 2
Comparison of the coordination anion–cation bond lengths and displacement energies for oxygen in various oxides

Material	Average no. of cations coordinated to oxygen sites (OCN)	Average anion–cation bond length[a] (Å)	E_d values measured by TRCS (eV)	Recommended[b] E_d values (eV)	Calculated[c] E_d values (eV)
CaO	6	2.4053	58 ± 2[d]		
MgO	6	2.1085	55 ± 2[d]	50	47.5
Al_2O_3	4	1.9139	58 ± 2[d]	50	43.3
Perovskite–$CaTiO_3$	4.67	2.2574	45 ± 4[e]		
Perovskite–$SrTiO_3$	6	2.4917	45 ± 4[e]		
Perovskite–$BaTiO_3$	6	2.5569	45 ± 4[e]		
Rutile TiO_2	3	1.9585	39 ± 4[f]		
Zirconolite $CaZrTi_2O_7$	4.1	2.1594	45 ± 4[f]		
Zircon $ZrSiO_4$	3	2.0124			53.1
Spinel $MgAl_2O_4$	4	1.9253		60	46.2
Pyrochlore $Y_2Ti_2O_7$	4	2.2016	47 ± 5[g]		
Pyrochlore $La_2Zr_2O_7$	4	2.3522	47 ± 5[g]		
Perovskite–$CaZrO_3$	4.67	2.3416	53 ± 5[g]		

[a] As calculated by 'CrystalMaker 5.0.1', a Mac based PC program for drawing and analysing crystallographic structures.
[b] Ref. [8].
[c] Ref. [20].
[d] Ref. [13].
[e] Ref. [9].
[f] Ref. [10].
[g] This study.

- the average cation–oxygen bond length (ABL) for each oxygen site
- E_d (oxygen) values as calculated by Williford et al. [20],
- some of the E_d (oxygen) values recommended by Zinkle and Kinoshita [8], and
- E_d (oxygen) values measured using TRCS determined in this and previous studies.

On the basis of the data for aluminium oxide (Al_2O_3), rutile (TiO_2) and spinel ($MgAl_2O_4$), the current authors previously suggested [10] that E_d (oxygen) in a compound correlated with its OCN. However this cannot be strictly true, as rutile (TiO_2) and zircon ($ZrSiO_4$) with the same OCN and similar ABLs have very different E_d (oxygen) values (39 and 53 eV respectively).

Some of the data in Table 2 suggest that the E_d (oxygen) of a compound is inversely related to the ABL of that compound. Specifically, Al_2O_3, $La_2Zr_2O_7$ and $Y_2Ti_2O_7$ all have OCNs of four; Al_2O_3 has an ABL of ~1.9 Å and E_d (oxygen) value of 58 eV; and $La_2Zr_2O_7$ and $Y_2Ti_2O_7$ have ABLs of ~2.25 Å and E_d (oxygen) values of 47 eV. However $SrTiO_3$ and $BaTiO_3$ have the same OCN (6), similarly different ABLs (~2.49 and 2.56 Å respectively) and the same E_d (oxygen) values of 45 eV.

On the basis of all the Table 2 data discussed above, there is no obvious correlation between the E_d (oxygen) value of a compound and its OCN or ABL.

Most of the titanates we have investigated using TRCS (perovskite, zirconolite and pyrochlore) are comprised of networks of corner-linked Ti–O octahedra and have E_d (oxygen) values of ~45 eV. Rutile (TiO_2) is comprised of both edge and corner-linked Ti–O octahedra and has an E_d (oxygen) value of 39 eV. The difference between the E_d (oxygen) value of rutile and the rest of the titanates is real and it may reflect the occurrence of edge-linked Ti–O octahedra in rutile or alternatively may be linked to the fact that TiO_2 can occur as various polytypes (rutile, brookite and anatase). Additionally or alternatively, the absence of additional binding cations compared with the other titanates may also contribute to more weakly bound oxygen anions.

Wang et al. [6] reported that $Gd_2Zr_2O_7$ pyrochlore could not be rendered amorphous by irradiation with 1 MeV Kr^+ ions (even at a dose was 10 times that required to render $Gd_2Ti_2O_7$ pyrochlore amorphous) and that irradiation caused the structure of $Gd_2Zr_2O_7$ to change from pyrochlore to fluorite. Consequently, it is interesting that the E_d (oxygen) values of $La_2Zr_2O_7$ and $Y_2Ti_2O_7$ are both 47 ± 5 eV, while the E_d (oxygen) values of $CaZrO_3$ and $CaTiO_3$ are 45 ± 4 and 53 ± 3 respectively. In combination, these results suggest that the difference between the radiation damage resistance of $Gd_2Zr_2O_7$ and $Gd_2Ti_2O_7$ may be due to differences in the displacement energies of the Zr and Ti in $Gd_2Zr_2O_7$ and $Gd_2Ti_2O_7$.

5. Conclusions

The TRCS measurements in this study have shown that: (a) the E_d (oxygen) in $La_2Zr_2O_7$ and zirconate perovskite are 47 ± 5, and 49 ± 5 eV respectively and (b) the E_d (oxygen) in zirconolite is 45 ± 5 eV.

Comparison of the data collected in this and previous studies suggests that E_d (oxygen) in all oxides lies between 39 and 58 eV and shows that the E_d (oxygen) does not correlate with either the coordination of the oxygen site or the average oxygen–anion bond length.

Acknowledgements

The authors thank Dr David Webb for both access to the ARPANSA LINAC and experimental assistance and Dr Gregory R. Lumpkin (formerly of ANSTO and currently of the University of Cambridge, UK) for constructive review.

References

[1] A.E. Ringwood, S.E. Kesson, N.G. Ware, W. Hibberson, A. Major, Nature (London) 278 (1979) 219.
[2] G.R. Lumpkin, J. Nucl. Mater. 289 (2000) 136.
[3] B.R. Meyers, G.A. Armantrout, C.M. Jantzen, A. Jostsons, L.M. McKibben, H.F. Shaw, D.M. Strachan, J.D. Vienna, Technical Evaluation Panel Summary Report, Plutonium Immobilisation Project, Report No. UCRL-ID-129315 (1998).
[4] I. Hayakawa, H. Kamizono, J. Mater. Sci. 28 (1993) 513.
[5] I. Hayakawa, H. Kamizono, J. Nucl. Mater. 202 (1993) 163.
[6] S.X. Wang, B.D. Begg, L.M. Wang, R.C. Ewing, W.J. Weber, K.V. Govidan Kutty, J. Mater. Res. 14 (1999) 4470.
[7] M.W.A. Stewart, B.D. Begg, E.R. Vance, K. Finnie, H. Li, G.R. Lumpin, K.L. Smith, W.J. Weber, S. Thevuthasan, Mat. Res. Symp. Proc. 713 (2002) 311.
[8] S.J. Zinkle, C. Kinoshita, J. Nucl. Mater. 251 (1997) 200.
[9] R. Cooper, K.L. Smith, M. Colella, E.R. Vance, M. Philips, J. Nucl. Mater. 289 (2001) 199.
[10] K.L. Smith, R. Cooper, M. Colella, E.R. Vance, Mater. Res. Soc. Symp. Proc. 663 (2001) 373.
[11] E. Sonder, W.A. Sibley, J.H. Crawford Jr., L.M. Slifkin, in: Point Defects in Solids, Vol. I, Plenum, New York, 1972, p. 201.
[12] B. Henderson, C.R.C Crit. Rev. Solid State Mater. Sci. 9 (1980) 1.
[13] K.J. Caulfield, R. Cooper, J.F. Boas, J. Am. Ceram. Soc. 78 (1995) 1054.
[14] B.D. Evans, M. Stapelbroek, Phys. Rev. B 18 (1978) 7089.

[15] E.A. Kotomin, R.I. Eglitis, G. Borstel, L. Grigorjeva, D. Millers, V. Pankratov, Nucl. Instrum. and Meth. B 166&167 (2000) 299.
[16] K.C. Humphreys, A.D. Kantz, Radiat. Phys. Chem. 9 (1977) 737.
[17] R.C. Powell, G.E. Venikouas, L. Xi, J.K. Tyminski, J. Phys. Chem. 84 (1986) 662.
[18] K.L. Smith, N.J. Zaluzec, R. Cooper, M. Colella, E.R. Vance, in: 10th International Ceramics Congress – Part A, P. Vincenzini (Ed.), Techna Srl. (2003) 15.
[19] W. Tam, R.N. Bhave, R. Cooper, D. Edmondson, Radiat. Phys. Chem. 45 (2) (1995) 187.
[20] R.E. Williford, R. Devanathan, W.J. Weber, Nucl. Instrum. and Meth. B 141 (1998) 94.